Featured Article

An N-Terminal Extension to UBA5 Adenylation Domain Boosts UFM1 Activation: Isoform-Specific Differences in Ubiquitin-like Protein Activation

Nadine Soudah[1], Prasanth Padala[1], Fouad Hassouna[1], Manoj Kumar[1], Bayan Mashahreh[1], Andrey A. Lebedev[2], Michail N. Isupov[3], Einav Cohen-Kfir[1] and Reuven Wiener[1]

1 - Department of Biochemistry and Molecular Biology, *The Institute for Medical Research Israel-Canada, Hebrew University–Hadassah Medical School, Jerusalem 91120, Israel*
2 - CCP4, *Research Complex at Harwell, STFC Rutherford Appleton Laboratory, Harwell Oxford, Didcot OX11 0FA, United Kingdom*
3 - The Henry Wellcome Building for Biocatalysis, *Biosciences, University of Exeter, Stocker Road, Exeter EX4 4QD, United Kingdom*

Correspondence to Reuven Wiener:
reuvenw@ekmd.huji.ac.il
https://doi.org/10.1016/j.jmb.2018.10.007
Edited by Titia Sixma

Nadine Soudah, Prasanth Padala, Fouad Hassouna and Reuven Wiener

Abstract

Modification of proteins by the ubiquitin-like protein, UFM1, requires activation of UFM1 by the E1-activating enzyme, UBA5. In humans, UBA5 possesses two isoforms, each comprising an adenylation domain, but only one containing an N-terminal extension. Currently, the role of the N-terminal extension in UFM1 activation is not clear. Here we provide structural and biochemical data on UBA5 N-terminal extension to understand its contribution to UFM1 activation. The crystal structures of the UBA5 long isoform bound to ATP with and without UFM1 show that the N-terminus not only is directly involved in ATP binding but also affects how the adenylation domain interacts with ATP. Surprisingly, in the presence of the N-terminus, UBA5 no longer retains the 1:2 ratio of ATP to UBA5, but rather this becomes a 1:1 ratio. Accordingly, the N-terminus significantly increases the affinity of ATP to UBA5. Finally, the N-terminus, although not directly involved in the E2 binding, stimulates transfer of UFM1 from UBA5 to the E2, UFC1.

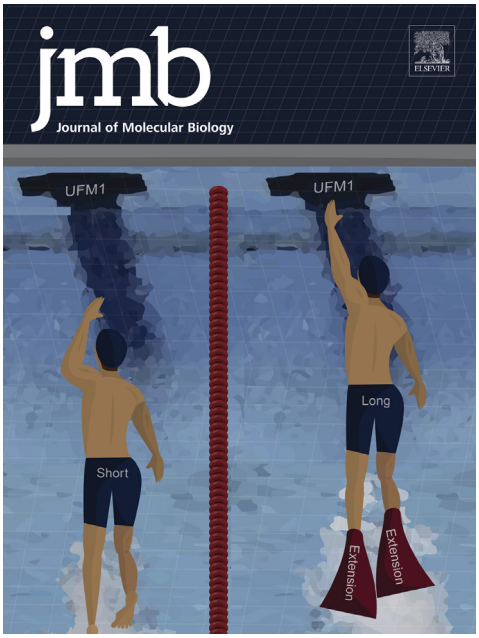

Legend: *The UFM1-activating enzyme, UBA5, possesses two isoforms: long and short. These isoforms are identical in their sequence except for an N-terminal extension, existing only in the long isoform. In this work, we solved the crystal structure of the long isoform, and deciphered the mechanism by which the N-terminal extension stimulates activation of UFM1.*

Introduction

Ubiquitin fold modifier 1 (UFM1) is a ubiquitin-like protein that shares the β-grasp fold of ubiquitin, although it has only 16% sequence identity with ubiquitin [1–3]. UFM1 is involved in several cellular processes, including endoplasmic reticulum homeostasis, erythropoiesis, fatty acid metabolism and cell division [4–11]. Moreover, protein modification by UFM1 (ufmylation) is associated with breast cancer and neurological disorders [12–16]. Notably, prevention of protein modification by UFM1 is embryonic lethal in mice due to severe anemia [17]. Similarly to ubiquitination, ufmylation is mediated through an enzymatic cascade involving E1, E2 and E3 enzymes [18–20]. First, the E1-activating enzyme, UBA5 (ubiquitin-like modifier-activating enzyme 5), binds ATP, magnesium and UFM1 and forms, upon the release of a pyrophosphate, an acyl adenylate intermediate. This intermediate is then subjected to attack by the UBA5 active-site Cys, and with the release of AMP, a high-energy thioester bond with UFM1 C-terminal glycine is formed. At that point, UFM1 is activated and ready to be transferred in a transthioesterification reaction from UBA5 to the active-site Cys of the E2, UFC1 (Ubiquitin-fold modifier-conjugating enzyme 1). Finally, in the presence of the E3, UFL1 (ubiquitin-fold modifier-protein ligase 1), UFM1 is transferred from UFC1 to a lysine residue on a target protein, forming an isopeptide bond [11,21–23].

UBA5 belongs to the non-canonical E1 enzymes that lack a defined Cys domain but have the active-site Cys within the adenylation domain [24]. Similar to other E1 enzymes, UBA5's adenylation domain comprises an eight-stranded beta sheet that is surrounded by helices [21]. Moreover, like the ancestral E1, MoeB, and the autophagy related E1, Atg7, the adenylation domain forms a homodimer with a pseudo-2-fold symmetry [25–28]. Besides the adenylation domain, both UBA5 and Atg7 possess a sequence outside the adenylation domain that is required for ubiquitin-like protein's binding. In UBA5, this sequence comprises 13 amino acids, which are known as the UFM1-interacting sequence (UIS) and are located C-terminal to the adenylation domain [2,29]. Previously, we and others have shown that the adenylation domain by itself is unable to activate UFM1, but a fragment possessing both the adenylation domain and the UIS successfully activates UFM1 [2,30]. Interestingly, although UBA5 dimerization is critical for UFM1 activation, UBA5 is not a stable dimer in solution. However, binding of UFM1 to UBA5 possessing the adenylation domain and the UIS stabilizes the dimeric state, which is needed for ATP binding and thereby for UFM1 activation [31]. Ultimately, in order to transfer UFM1 to UFC1, UBA5 contains a short sequence at the C-terminus that is required for UFC1 binding [32].

Human UBA5 has two isoforms, each including the above-mentioned three regions: the adenylation domain, UIS and UFC1-binding sequence [1,33]. However, only one has an extension of 56 amino acids N-terminal to the adenylation domain (Fig. 1a). Previously, we and others have shown that the short isoform (without the first 56 amino acids) satisfies activation of UFM1 as well as transfer of UFM1 to UFC1 [21,34]. This suggests that the 56 amino acids N-terminal to the adenylation domain are not essential for UBA5 function, therefore raising the question of their role in UBA5's function. Here we provide structural and biochemical data on the UBA5 N-terminus in order to understand its contribution to UFM1 activation. The crystal structures of the UBA5 long isoform bound to ATP with and without UFM1 show, for the first time, that the N-terminus not only is involved in ATP binding but also affects how the adenylation domain interacts with ATP. This leads to the ATP gamma-phosphate adopting a different position to that in the structure of the short isoform. Moreover, the active-site Cys, which in the short isoform resides on one of the adenylation domain helices, is now moved to the crossover loop. Surprisingly, in the presence of the N-terminus, the 1:2 ratio of ATP to UBA5 is not retained but becomes 1:1. Accordingly, the N-terminus significantly increases the affinity of ATP to UBA5, thereby facilitating UFM1 activation at low ATP concentrations. Finally, the N-terminus, although is not directly involved in UFC1 binding, stimulates transfer of UFM1 from UBA5 to UFC1. Taken together, our results provide the structural mechanism for the role of the UBA5 N-terminus in UFM1 activation.

Results and Discussion

The N-terminus of UBA5 facilitates UFM1 activation

Although UBA5 lacking the N-terminus (amino acids 1–56) satisfies activation of UFM1, we were interested to know if the N-terminus contributes to UFM1 activation. To that end, we compared the activation of UFM1 by UBA5 1–347 (hereafter referred to UBA5) and UBA5 57–346. As expected, both forms successfully activated UFM1 (i.e., generation of UBA5~UFM1 adduct), but activation was significantly faster with UBA5 possessing the N-terminus. Specifically, in the presence of the N-terminus, most of the activation process occurred within the first half a minute, while in its absence, it lasted more than 10 min (Fig. 1b). Since these experiments were performed with 5 mM ATP (a concentration used to characterize the short UBA5 isoform [34]), we also compared activation at 10 μM ATP. After 10 min, activation of UFM1 was observed only with UBA5 possessing the N-terminus (Fig. 1b). Surprised by the ability of UBA5 possessing

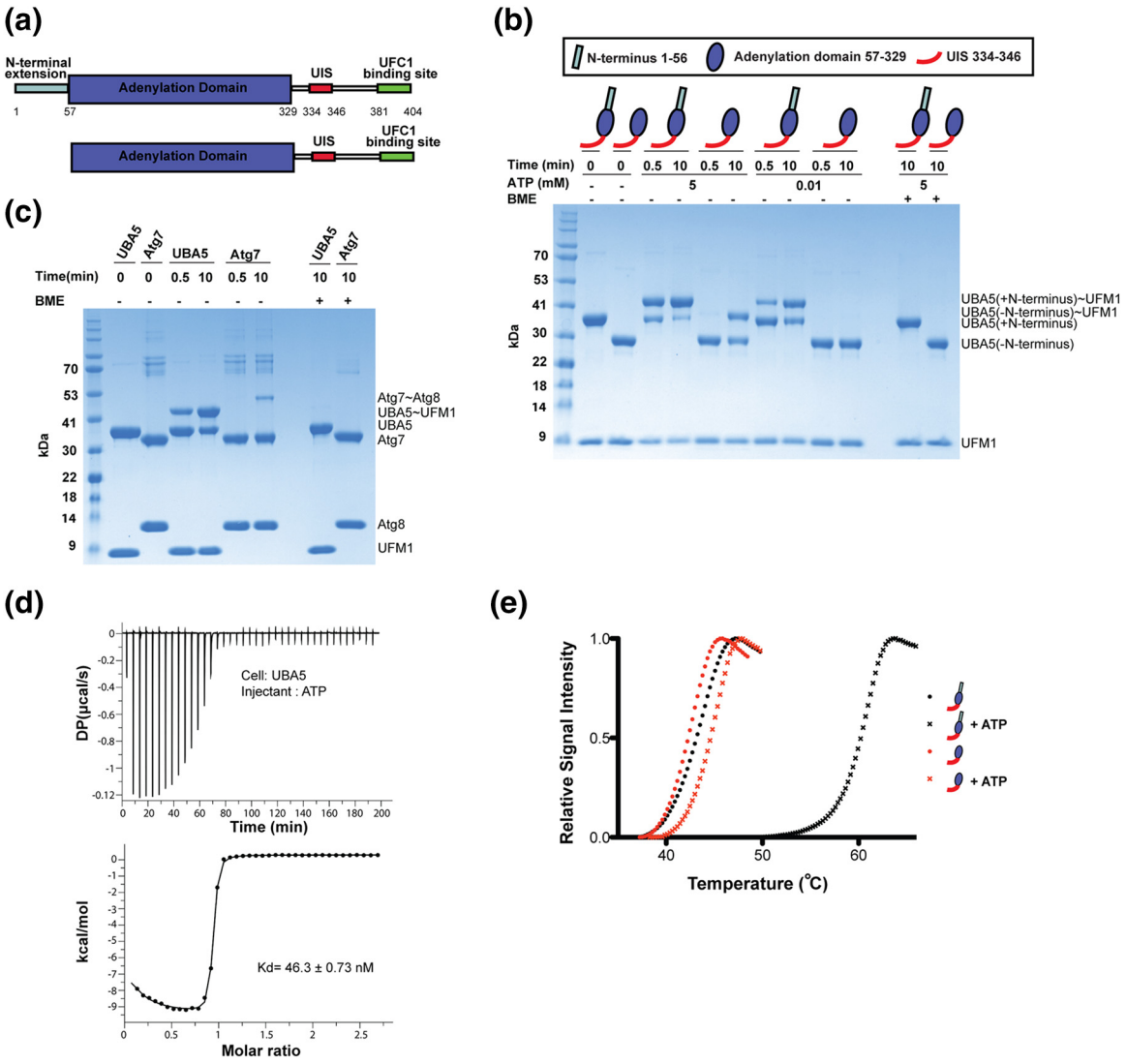

Fig. 1. UBA5's N-terminus stimulates UFM1 activation by enhancing ATP binding. a, Schematic representation of UBA5 isoforms with and without the N-terminal extension. b, Activation of UFM1 (20 µM) by UBA5 with and without the N-terminus (10 µM) at 5 mM and 10 µM ATP concentrations. c, Charging assay of UBA5 possessing the N-terminus (10 µM) or Atg7 (10 µM) with UFM1 (20 µM) or Atg8 (20 µM) at 10 µM ATP. d, ITC experiment of ATP binding to UBA5 possessing the N-terminus. Top panel shows raw data of heat flow *versus* time for titrating 1 mM ATP into buffer containing 75 µM UBA5. The area under the peaks of the upper panel was integrated and plotted as kcal per mole of ATP as a function of binding stoichiometry in the bottom panel. Thermodynamic parameters are summarized in Supplemental Table S1. e, TSA of UBA5 with and without the N-terminus in the presence and absence of 5 mM ATP. Each experiment was performed in triplicate, and the melting curves show the average normalized to relative signal intensity as a function of temperature. Denaturation midpoints are summarized in Supplemental Table S2.

the N-terminus to activate UFM1 at a very low ATP concentration, we then asked whether the other non-canonical E1 enzyme, Atg7, also has this ability. As shown in Fig. 1c, after 30 s, we obtained activation of UFM1 but failed to detect any activation of Atg8 by Atg7. Taken together, our results suggest that in the presence of the N-terminus, UBA5 can activate UFM1 at a low concentration of ATP.

UBA5 N-terminus plays a role in ATP binding and protein thermal stability

The ability of only UBA5 possessing the N-terminus to activate UFM1 at low ATP concentrations suggests that the N-terminus contributes to the binding of ATP to UBA5. To test this possibility, we measured the affinity of ATP to UBA5 using ITC (Fig. 1d and

Table S1). The ITC data were best fitted with a two binding sites model, although only one site possessed a meaningful ratio of ATP to UBA5 (the other binding site we considered as nonspecific since it has a ratio of 1:141 ATP to UBA5). The measured K_d value was in the nanomolar range (46 nM) and was 3 orders of magnitude lower than the K_d value obtained for the binding of ATP to UBA5 57–346 [31], suggesting that the N-terminus of UBA5 is involved in ATP binding. We next tested whether the N-terminus plays a role in the stability of UBA5. As shown in Fig. 1e and Table S2, the above two constructs of UBA5 possess a similar thermal stability with denaturation midpoints of ~42.5 °C. However, in the presence of 5 mM ATP, UBA5 demonstrated a 17 °C increase in the denaturation midpoint, while UBA5 57–346 had an increase of only 2.4 °C. Taken together, these results suggest that binding of ATP to UBA5, which is facilitated by the N-terminus, significantly increases the thermal stability of UBA5.

Previously, we have shown that the UIS is needed not only for UFM1 binding but also for increasing UBA5's affinity to ATP [2,31]. Specifically, binding of UFM1 to the UIS stabilizes the dimeric state of UBA5, and this enhances the affinity of UBA5 to ATP. Accordingly, removing the UIS from the short UBA5 isoform prevented activation of UFM1 [2]. This prompted us to ask whether in the long UBA5 isoform, which possesses high affinity to ATP, removing the UIS has a deleterious effect. To that end, we tested UFM1 activation by UBA5 1–335 that possesses the N-terminus but lacks the UIS. As shown in Fig. 2a, removing the UIS did not abolish the activation of UFM1 by UBA5 possessing the N-terminus. This unexpected result further suggests that in the short isoform, removing the UIS prevents activation due to a failure in ATP, but not in UFM1, binding to UBA5. Interestingly, a decrease in the binding affinity of the ubiquitin E1, UBA1, to ATP shifts the mechanism of substrate binding from pseudo-ordered to a purely random mechanism [36,37], thereby raising the possibility that UBA5 N-terminus, which enhances affinity to ATP, plays a role in the mechanism of substrate binding.

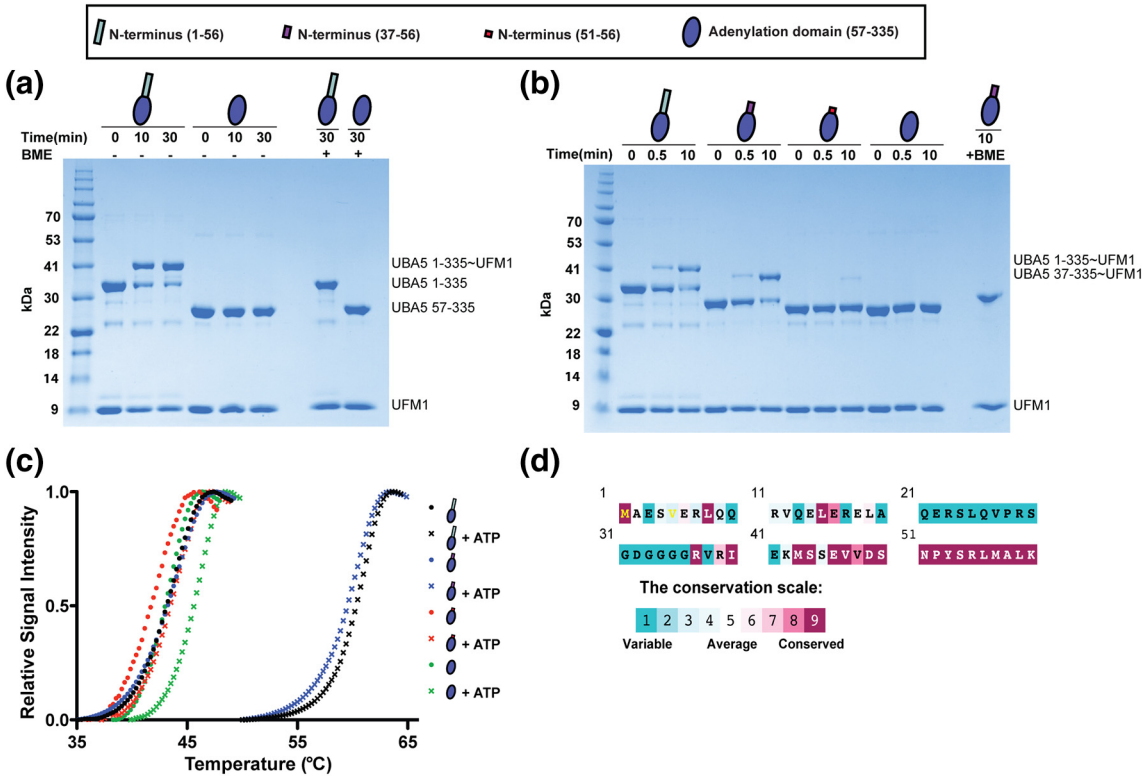

Fig. 2. Characterizing the ability of UBA5's N-terminus to rescue UFM1 activation in the absence of the UIS. a, Activation of UFM1 (20 μM) by UBA5 with and without the N-terminus in the absence of the UIS (10 μM) at 5 mM ATP. b, Mapping the N-terminus of UBA5 by activation assay at 10 μM ATP. All constructs end at amino acid 335 (–UIS) and start as indicated in the figure. c, Mapping the N-terminus of UBA5 lacking the UIS by TSA. Melting temperature of UBA5 constructs was obtained in the absence and presence of 5 mM ATP. Each experiment was performed in triplicate, and the melting curves show the average normalized to relative signal intensity as a function of temperature. Denaturation midpoints are summarized in Supplemental Table S2. d, ConSurf evolutionary conservation analysis of UBA5's N-terminus [35]. The N-terminus residues of UBA5 are colored according to their conservation score.

The difference between the above two UBA5 constructs that lack the UIS is the extension of 56 amino acids located N-terminal to the adenylation domain that exists only in one construct. To investigate whether the intact N-terminus (i.e., amino acids 1–56) is required for facilitating ATP binding and subsequently stimulating UFM1 activation by UBA5, we generated two UBA5 constructs that start at amino acid 37 or 51 and end at amino acid 335. As shown in Fig. 2b, removing the first 36 amino acids, but not the first 50, did not affect the ability of UBA5 to activate UFM1. Accordingly, while UBA5 (37–335) had the same thermal stability as UBA5 possessing the full N-terminus (1–335), UBA5 (51–335) demonstrated not only a lower denaturation midpoint in the absence of ATP but also a shift of only 1.9 degrees in the presence of ATP (Fig. 2c and Table S2). These results are in line with the conservation score of the UBA5 N-terminal amino acids, whereby the first 36 amino acids are weakly conserved, whereas the amino acids from 37 are highly conserved (Fig. 2d). Taken together, our results suggest that the contribution of the UBA5 N-terminus to UFM1 activation, ATP binding and thermal stability is mediated via amino acids 37–56 and does not require the first 36 amino acids of UBA5.

The N-terminus of UBA5 contributes to the transfer of UFM1 from UBA5 to UFC1

Although the only step in UFM1 conjugation that requires energy is UFM1 activation by UBA5, ATP also plays a role in the transfer of UFM1 from UBA5 to UFC1. Specifically, Gavin *et al*. [38] have shown that charged UBA5 (UBA5 ~ UFM1) hardly transfers UFM1 to UFC1 if ATP is missing. In that case, hydrolysis of ATP is not required but only binding of ATP to the UBA5 ~ UFM1 adduct. This connection between ATP binding and transfer of UFM1 to UFC1 prompted us to test whether the N-terminus of UBA5 plays a role in this transfer. To that end, we charged UBA5 long and short isoforms with UFM1. In that step, we ensured that at the end of the reaction there is no free UFM1 left (Fig. 3a, lanes 3 and 9). We then added UFC1 and looked for charging of UFC1 with UFM1. Thereby, differences in UFC1 charging between the UBA5 isoforms were only due to UFM1 transfer from UBA5 to UFC1 and were not affected by the rate of UFM1 activation by the UBA5. As shown in Fig. 3a, the charging of UFC1 with UFM1 was significantly better in the case of the long UBA5 isoform, thereby suggesting that the presence of the N-terminus contributes to UFM1 transfer to UFC1. Next, to further characterize the role of the N-terminus in UFM1 transfer to UFC1, we tested whether the N-terminus is involved in the binding of UBA5 to UFC1. To that end, we performed an ITC experiment with UFC1 and the above UBA5 isoforms. As shown in Fig. 3b and c and Table S1, both isoforms of UBA5 bind UFC1 with a similar affinity (K_d of ~ 1 μM), suggesting that the N-terminus does not contribute to the UFC1 binding. We then asked whether the effect of the N-terminus on UFM1 transfer is coupling to ATP binding. Previously, we showed that only in the presence of the N-terminus does ATP significantly stabilize UBA5 (Fig. 1d and Table S2). This therefore prompted us to test whether ATP has similar effect when UBA5 is already charged with UFM1. To overcome the instability of the thioester bond, we exploited the cross-linker bis-maleimidoethane (BMOE), which has successfully been used with other E1 enzymes [39], and generated a stable adduct of UBA5 ~ UFM1 (G83C). Then, using the thermal shift assay (TSA), we tested the effect of ATP on the stability of the charged long or short UBA5 isoform. As shown in Fig. 3d and Table S2, in the adduct comprising the long isoform, ATP increased the thermal stability by 12 °C. However, with the short isoform, no increase in thermal stability was observed, rather an unexpected decrease of 2.2 °C. This therefore suggests that upon ATP binding to UBA5 ~ UFM1, the N-terminus undergoes conformational changes that stabilize the adduct and facilitates faster UFM1 transfer to UFC1. Interestingly, binding of ATP to the ubiquitin E1, UBA1, has been shown to enhance the affinity of the latter to the E2, which in turn stimulates the rate of ubiquitin adenylate formation [36].

Crystal structures of UBA5 possessing the N-terminus bound to ATP and Mg with and without UFM1

To date, while crystal structures of UBA5 bound to ATP or in complex with UFM1 have already been solved, they all comprise the short UBA5 isoform, thereby lacking the first 56 amino acids [21,34]. Moreover, in these structures, amino acids 57–68, although existing in the crystals, are not observed in the structure. Therefore, to obtain structural insight into to the role of UBA5 N-terminus in UFM1 activation, we determined the crystal structure of UBA5 (37–335) bound to ATP and Mg at 2.7-Å resolution (Table S3). Crystals of UBA5 (37–335) bound to ATP contained 16 molecules of UBA5, each bound to one ATP molecule, in the $P2_1$ asymmetric unit. Superposition of the 16 UBA5 molecules in the ASU yields RMSD values lower than of 0.15 Å, suggesting no significant structural differences between the molecules. The 16 UBA5 molecules are arranged in eight dimers, and each dimer has the same pseudo-2-fold symmetry axis (Fig. 4a). We also determined the crystal structure of UBA5 (37–347) in complex with ATP, Mg and UFM1 at 2.1-Å resolution (Table S3). This structure comprises UBA5 that ends at amino acid 347 and therefore includes the UIS, which facilitates binding to UFM1. In addition, to prevent activation of UFM1 by UBA5, we used UFM1

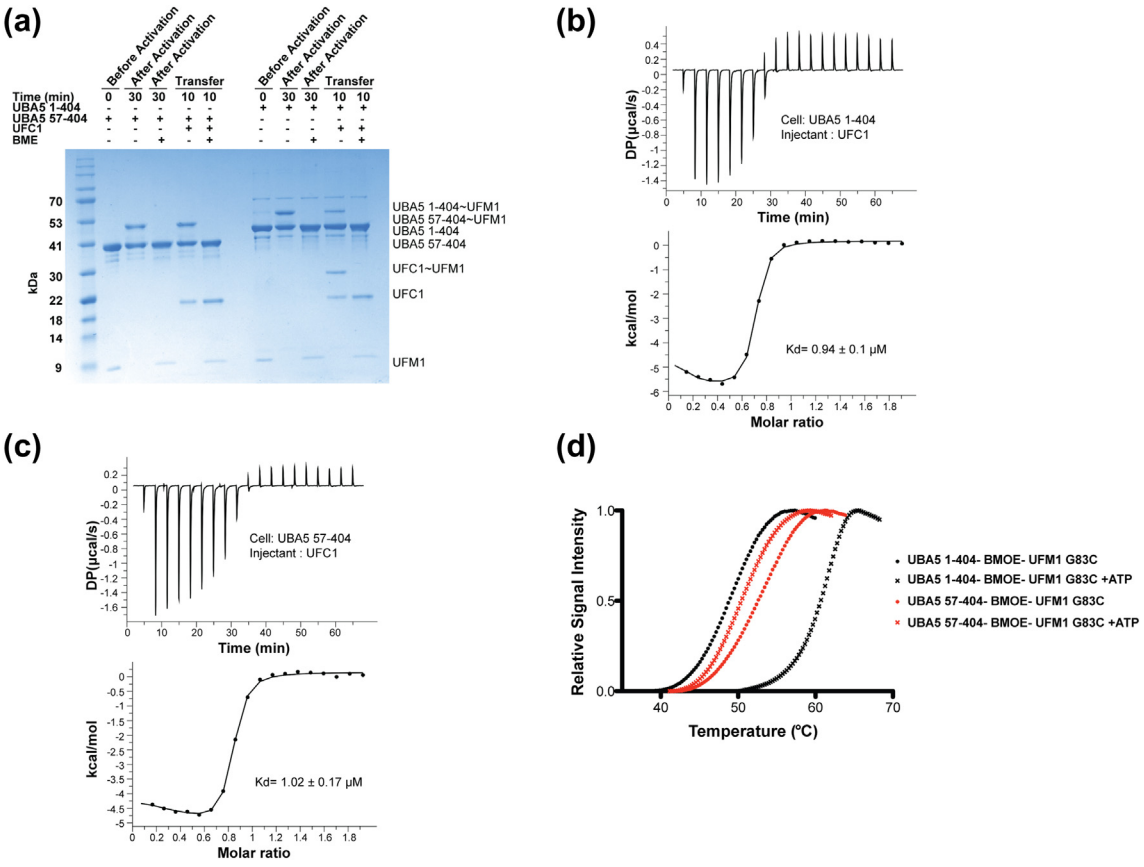

Fig. 3. The role of UBA5's N-terminus in UFC1 charging. a, Transfer assay of UFM1 from UBA5 to UFC1. UFC1 was added to pre-formed UBA5 ~ UFM1. b, ITC experiment of UFC1 binding to UBA5 1–404. Top graph represents raw data of heat flow *versus* time for titrating 2.4 mM UFC1 into buffer containing 239 µM UBA5. The exothermic peaks are due to UFC1 binding to UBA5, while the endothermic peaks appear after saturation of UFC1 binding to UBA5 and are due to buffer mismatch. The area under the peaks of the upper panel was integrated and plotted as kcal per mole of UFC1 as a function of binding stoichiometry in the bottom panel. Thermodynamic parameters are summarized in Supplemental Table S1. c, As in panel B, but UFC1 binding to UBA5 57–404 instead of UBA5 1–404. d, TSA of UBA5 1–404 or UBA5 57–404 cross-linked to UFM1 G83C in the absence and presence of 5 mM ATP. Each experiment was performed in triplicate, and the melting curves show the average normalized to relative signal intensity as a function of temperature. Denaturation midpoints are summarized in Supplemental Table S2.

that lacks the last 4 amino acids (UFM1ΔC). This structure therefore represents the complex prior to UFM1 adenylation by UBA5. Crystals contained four molecules of UBA5, four molecules of UFM1ΔC and four molecules of ATP in the $P2_1$ asymmetric unit. The four UBA5 molecules in the ASU formed two homodimers, while each dimer bound two molecules of UFM1 and ATP (Fig. 4b). Superposition of the two dimers yielded an RMSD of 0.135 Å suggesting no significant structural difference between the dimers. However, in one UBA5 molecule, the first 7 amino acids acquired a different position than the one observed for these residues in the other three UBA5 molecules. This suggests that amino acids 36–42 are flexible and their structure is probably affected by crystal packing.

Superposition of the two UBA5 structures with and without UFM1 shows that the structural differences in UBA5 upon UFM1 binding are concentrated in the crossover loop (Fig. 4c). These structures, in contrast to the structures of UBA5 short isoform, have clear electron density for the entire UBA5 crossover loop, suggesting that the N-terminus assists in stabilizing this loop both in the absence or presence of UFM1. The movement of the crossover loop upon UFM1 binding is critical for preventing clashes with UFM1 and to enable UFM1 reaching the UBA5 active-site Cys. Intriguingly, although the crossover loop undergoes major conformational changes upon UFM1 binding, the position of the active-site Cys250, which resides on that loop, is not affected by the presence or absence

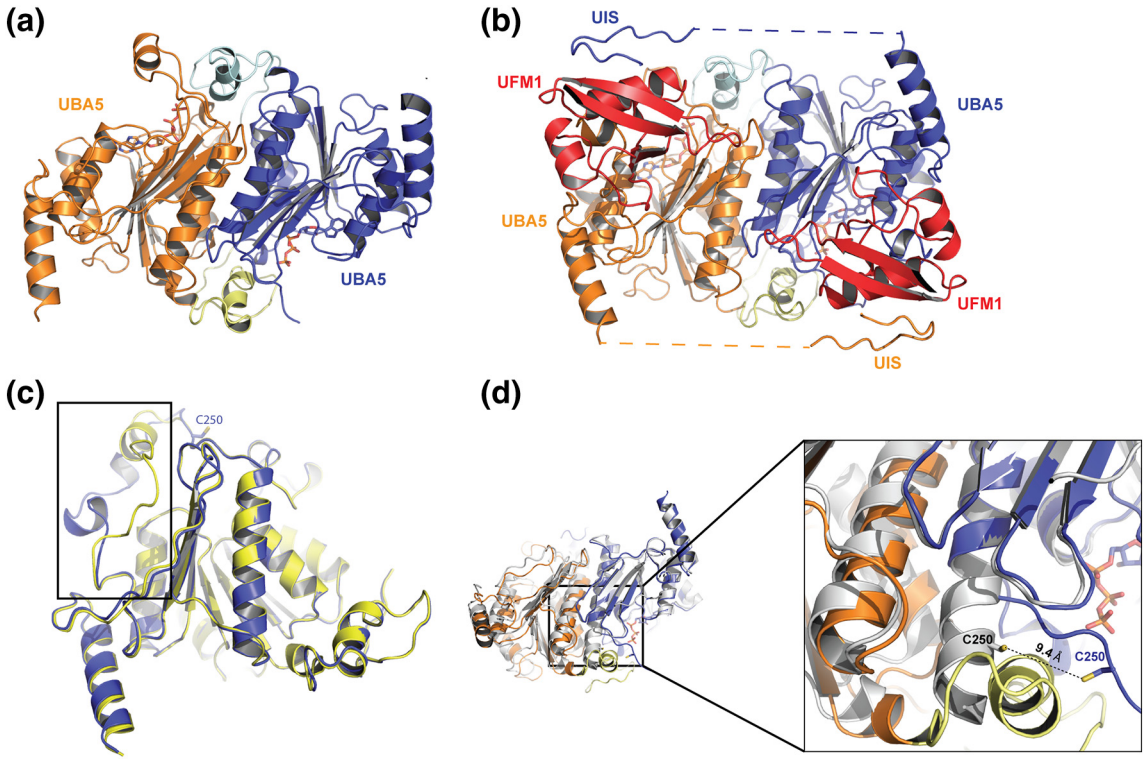

Fig. 4. Schematic representations of the crystal structures of UBA5 long isoform. a, The UBA5 homodimer: the N-termini of the orange and blue subunits are colored in yellow and cyan, respectively. Each UBA5 subunit binds ATP. b, The complex of UBA5–UFM1: UBA5 is depicted as in panel A; UFM1 is colored red. c, Superposition of UBA5 alone (yellow) with UBA5 in complex with UFM1 (blue). The main structural changes in UBA5 due to UFM1 binding are concentrated in the crossover loop (indicated by a rectangle). d, Superposition of UBA5 short isoform (gray) with UBA5 long isoform (colored as in panel A). In the short isoform, the helix comprising the active-site C250 overlaps with the N-terminus of the long isoform. Indeed, in the long isoform, this helix is shorter and the active-site Cys is ~9 Å away from its position in the short isoform.

of UFM1 (Fig. 4c). This does not hold true with the short UBA5 isoform where the presence of UFM1 alters the position of Cys250 [21,34].

Structural insight into UBA5 N-terminus

While the N-terminus contributes to UFM1 activation, it is not in direct contact with the UFM1 that is bound to UBA5 adenylation domain (Fig. 4b). Accordingly, superposition of the UBA5 N-terminus (amino acids 43–68) from the structures with and without UFM1 yields an RMSD of 0.146 Å, suggesting that the presence of UFM1 does not alter the structure of the N-terminus. The overall structure of the N-terminus appears as a bulge outside the adenylation domain that faces toward the adenylation domain of the other protomer (Fig. 4a and b). Superposition of the UBA5 long isoform with the short isoform shows that the N-terminus overlaps with the position of the adenylation domain's helix that comprises the active-site Cys250 (Fig. 4d). Accordingly, in the structure of the long isoform, this helix is shorter and thereby leaves room for the N-terminus that occupies this space. This results in a rearrangement in the position of the active-site Cys250, which no longer resides in helix but in the crossover loop. This resembles the position of Atg7 active-site Cys that also resides within the crossover loop [27].

The N-terminus forms a network of intramolecular interactions (Fig. 5a). These interactions include Asp49 and Lys60 that form salt bridges with Arg55 and Glu69, respectively. In addition, Tyr53 forms cation–pi interaction, aromatic sulfur interaction and hydrogen bond with Arg72, Met43 and Asn139, respectively. These interactions are accompanied by a set of hydrophobic interactions that include the N-terminal residues Ile64 and Val65 and the adenylation domain residues Leu274, Phe276. The N-terminus also has intermolecular interactions with the adenylation domain of the other protomer (Fig. 5b). Leu56, Ala58 and Leu59 and Met62 form hydrophobic interactions with the crossover loop residues Ala252, Leu254 and Pro255. The N-terminus also interacts with the adenylation domain's loop comprising amino acids 103–127. Clear electron density for that loop was not obtained in any crystal

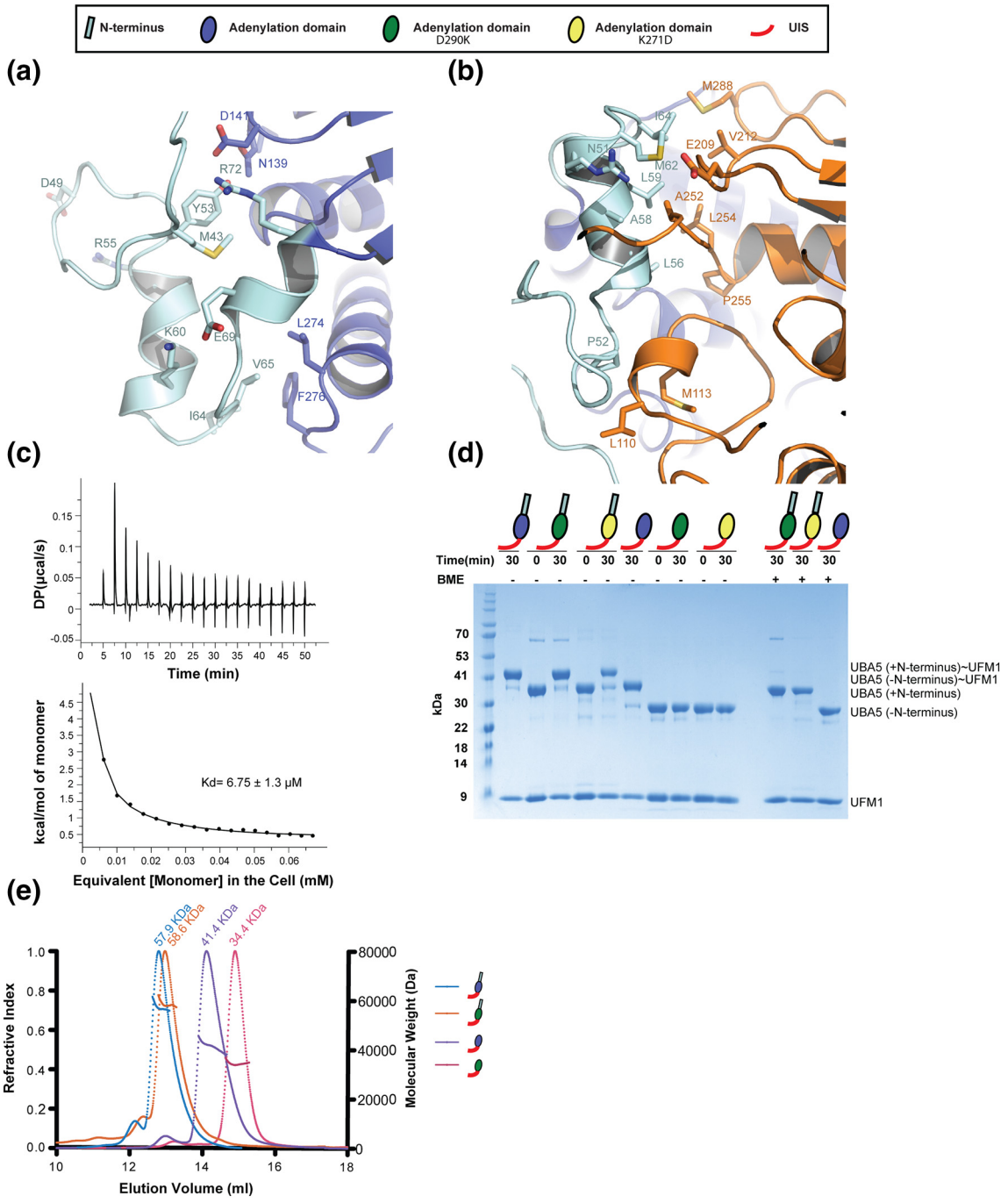

Fig. 5. Structural insights into UBA5's N-terminus. a, Intramolecular interactions of UBA5 N-terminus (cyan) with the adenylation domain (blue). b, Intermolecular interactions of UBA5 N-terminus (cyan) with the adenylation domain of the protomer (orange). c, ITC experiment of UBA5 disassociation. Top panel shows the raw data of heat change against time for the titration of UBA5 into buffer. Bottom panel shows the enthalpy change against the equivalent UBA5 monomer concentration. Thermodynamic parameters are summarized in Supplemental Table S4. d, Activation of UFM1 by UBA5 constructs (containing or lacking N-terminus) in the presence and absence of dimerization mutations (D290K or K271D) at 5 mM ATP. e, Size exclusion chromatography with multi-angle light scattering analysis of UBA5 constructs (containing or lacking N-terminus) in the presence and absence of dimerization mutation (D290K). Refractive index and molar mass are plotted against elution volume. The line under each peak corresponds to the average molecular mass determined by multi-angle light scattering, and the molecular weight of each construct is indicated above the peak and colored accordingly.

structure of the short isoform, suggesting that in the absence of the N-terminus, this loop is highly flexible. In that loop, Leu110 and Met113 form hydrophobic interactions with Pro52 of the N-terminus.

The structural data suggesting that the N-terminus interacts with the other protomer of the UBA5 dimer prompted us to test whether these interactions affect the stability of the UBA5 homodimer. As shown in Fig. 5c and Table S4, in an ITC experiment, we obtained a K_d of 6.8 μM for UBA5 dimerization. This value is 5-fold lower than the one measured for the short isoform [31], suggesting that the N-terminus contributes to the stability of the UBA5 homodimer. Previously, we showed that the dimerization mutants K271D and D290K of the short UBA5 isoform prevent activation of UFM1 by decreasing dimer formation [34]. We therefore asked whether in the context of the long isoform, which is more stable, these mutations have a similar effect. As shown in Fig. 5d, these mutants did not prevent activation of UFM1, suggesting that these mutations in the background of the long isoform are not as deleterious as in the context of the short isoform. This finding prompted us to investigate whether the D290K mutation in the context of the long isoform affects UBA5 dimer formation. Using size exclusion chromatography with multi-angle light scattering, we tested the molecular weight of UBA5 WT and D290K containing and missing the N-terminus. As shown in Fig. 5e, UBA5, WT or D290K that has the N-terminus yielded a similar molecular weight of (~58 kDa). However, the same mutation in the context of UBA5 that lacks the N-terminus yielded a molecular weight of 34 kDa, which is lower than the measured molecular weight of WT UBA5 that lacks the N-terminus (41 kDa). Taken together, our results suggest that the dimerization mutation in the context of UBA5 possessing the N-terminus hardly affects the dimer stability of UBA5, therefore enabling the activation of UFM1.

Structural insight into ATP binding in UBA5 long isoform

Our crystal structures provide not only insight into the structure of UBA5 N-terminus but also an understanding of how the UBA5 long isoform binds ATP. Although the ATP-binding pocket of UBA5 is located within the adenylation domain, which exists in the short isoform, our structure reveals that the N-terminus contributes to ATP binding. The N-terminus of one protomer directly interacts with the ATP that sits in the adenylation domain of the other UBA5 promoter (Fig. 6a). This is achieved via Arg55 of the N-terminus that contacts the gamma-phosphate oxygen atom of ATP. Arg55 resembles Arg14 of the ancestral homodimeric E1, MoeB, which binds the ATP that is bound to the adenylation domain of the other protomer [26]. Of note, such an Arg is missing in the non-canonical E1, Atg7, but exists in the heterodimeric E1s of SUMO (Sae2/Sae1) and NEED8 (APPBP1/UBA3) [40]. In the E1 of SUMO, Arg21 of Sae1 interacts with the ATP that is bound to the Sae2 adenylation domain. Similarly, in the E1 of NEED8, Arg15 of APPBP1 generates a salt bridge with the ATP gamma-phosphate [41]. To validate the importance of Arg55 in UFM1 activation, we tested activation of UFM1 by UBA5, R55A. Indeed, as shown in Fig. 6b, this mutation reduced UFM1 activation. In addition, in contrast to WT UBA5, this mutation prevented the increment in UBA5's thermal stability in the presence of ATP (Fig. 6c and Table S2). Next, to further characterize the role of Arg55 in activation, we performed an ITC experiment to measure the affinity of UBA5 R55A to ATP (Fig. 6d and Table S1). Similar to the WT protein, although the ITC data were best fitted to a two binding sites model, only one site had a meaningful ratio of ATP to UBA5. This binding site had a K_d of 1.7 μM that is 36-fold higher than the K_d of ATP to WT UBA5, suggesting that the R55A perturbs binding of ATP to UBA5. Of note, UBA5 with an R55H mutation has been recently reported for individuals with severe infantile-onset encephalopathy [14].

The presence of the N-terminus not only contributes an additional interaction with ATP but also alters how the adenylation domain binds the ATP. Both UBA5 isoforms have a network of hydrophobic interactions between the adenylation domain and ATP. This network includes Gly83, Gly82, Cys181, Gly80, Ala187, Val182 and Ile151 of the adenylation domain that are in contact with ATP. However, in contrast to this network, which is hardly affected by the N-terminus, significant differences are observed in the hydrogen bonds and salt bridges that each UBA5 isoform generates with ATP. In the short UBA5 isoform, the hydrogen bonds, formed by the adenylation domain, are concentrated in two residues. Specifically, Lys127 binds the ATP ribose and gamma-phosphate oxygen atom, and Asn184 binds the adenine (PDB code; 3H8V). However, in the long isoform, the adenine forms a hydrogen bond not only with Asn184 but also with the side chain of Asn150 and with the backbone nitrogen of Ile151 (Fig. 6a). In parallel, Lys127 retains its interaction with the ribose, but instead of binding the gamma-phosphate oxygen, as in the short isoform, it binds the beta-phosphate oxygen. In addition, Arg115 that is not observed in the short isoform crystal structure due to high flexibility forms salt bridges with the α–β–γ phosphate oxygen atoms of the ATP. This Arg corresponds to Arg73 of MoeB, Arg59 of Sae2 or Arg90 of UBA3 that forms a salt bridge with ATP. Interestingly, although Atg7 possesses Arg366 at a similar position to that of Arg115 in UBA5, this Arg is not involved in ATP binding. In contrast to the R55A mutation that had little effect on UFM1 activation, R115A totally abolished activation (Fig. 6e).

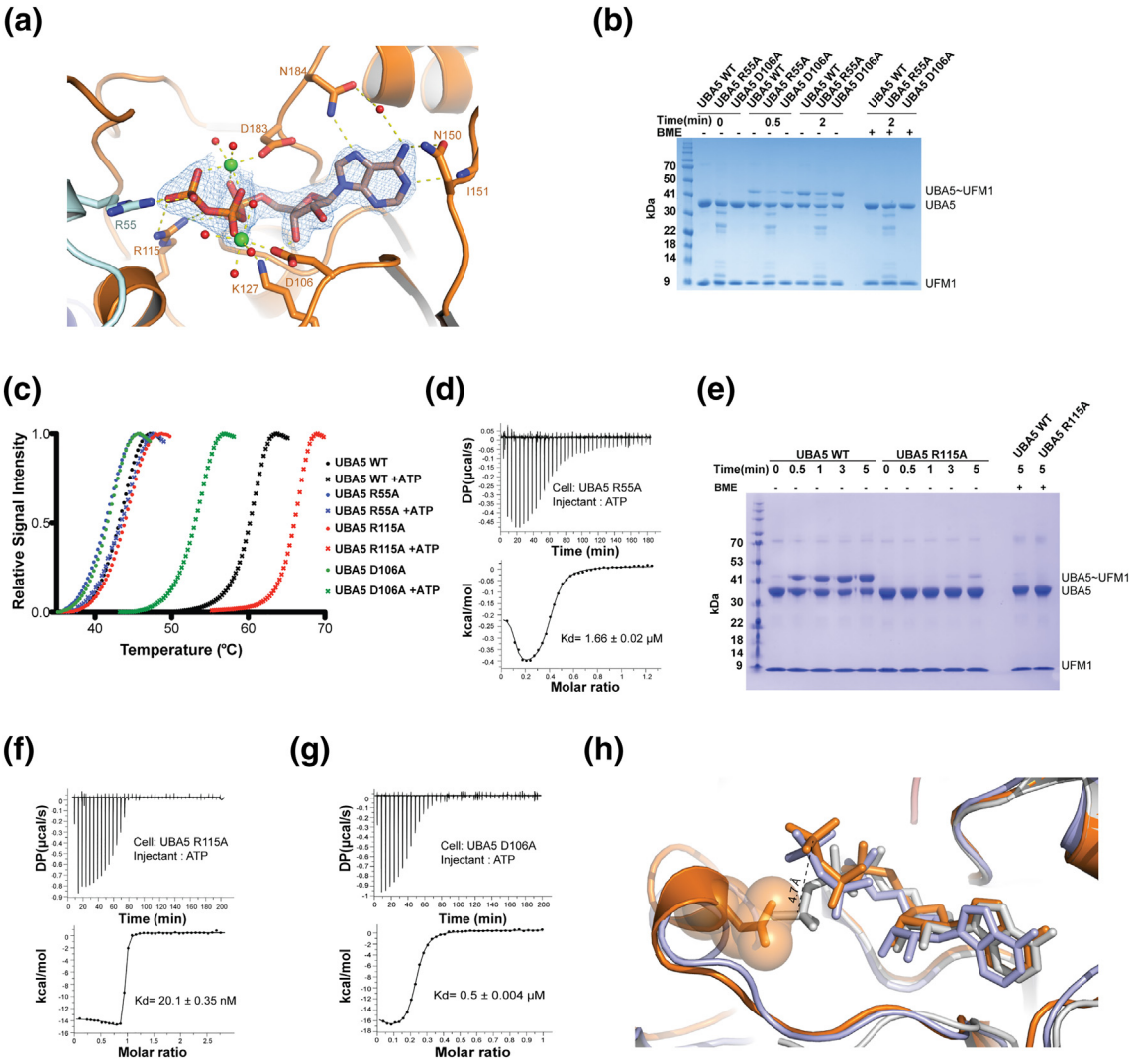

Fig. 6. Structural insights into the ATP binding region of UBA5. a, ATP bound to UBA5. ATP interacts with the adenylation domain of one UBA5 protomer (orange) and with the N-terminus of the other protomer (cyan). Side chain of residues involved in ATP binding is indicated. ATP is shown in the stick representation, together with an electron density map contoured at 1.0σ. b, Activation of UFM1 (20 µM) by UBA5 WT or mutants (10 µM) at 10 µM ATP. Thioester bond formation was monitored over time and stopped with sample buffer containing or lacking BME. c, Melting curves of UBA5 WT and mutants in the absence and presence of 5 mM ATP. Melting curves show the relative signal intensity as a function of temperature obtained from triplicates. Denaturation midpoints are summarized in Supplemental Table S2. d, ITC experiment checking ATP binding to UBA5 R55A. ATP (1 mM) was titrated into buffer containing 150 µM UBA5 R55A. Top graph displays the raw data of heat against time, and the bottom graph represents the enthalpy change *versus* the molar ratio of ATP to UBA5 R55A. Thermodynamic parameters are summarized in Supplemental Table S1. e, Activation assay of UBA5 R115A (10 µM) in comparison to UBA5 WT (10 µM) with UFM1 (20 µM) at 10 µM ATP. f, As in panel D, but with 0.5 mM ATP and 35 µM UBA5 R115A instead of UBA5 R55A. g, As in panel D, but with 0.5 mM ATP and 100 µM UBA5 D106A instead of UBA5 R55A. h, Superposition of UBA5 long isoform (orange) short isoform (gray) and Atg7 (cyan), each bound to ATP. ATP from each structure is shown in the stick representation.

Surprisingly, the ITC experiment showed that this mutation does not affect the affinity of ATP to UBA5 (K_d = 20 nM) (Fig. 6f and Table S1). In addition, this mutation, in contrast to R55A, does not prevent the increment of UBA5 thermal stability in the presence of ATP. As shown in Fig. 6c and Table S2, in the presence of ATP, the thermal stability of UBA5 R115A increased by 22 °C. This therefore suggests that Arg115 is not critical for ATP binding but instead has a catalytic role that is essential for UFM1 activation.

Similar to other E1 enzymes, binding of Mg to UBA5 is critical for ATP binding and UFM1 activation. While the short UBA5 isoform was crystalized in

the presence of ATP and Mg, its crystal structure contained ATP but not Mg (PDB ID; 3H8V). Surprisingly, our structures have two Mg ions per ATP molecule. One Mg ion is coordinated with ATP alpha-, beta- and gamma-phosphate oxygen atoms, the side chain of Asp183 and two water molecules that together generate an octahedral geometry (Fig. 6a). Asp183 is highly conserved and corresponds to Asp130 of MoeB, Asp117 of Sae2, Asp146 of UBA3 or Asp438 of Atg7. The other Mg generates octahedral geometry with the beta-phosphate oxygen atom, Asp106 and four water molecules (Fig. 6a). Of note, this Asp is missing in Atg7, but although it exists in MoeB and Sae2 as Asp64 and Asp50 respectively, these E1 structures lack the Mg ion bound to these aspartates. On the contrary, in the structure of the canonical E1, Uba1 (PDB ID; 4II2), Asp 465, which corresponds to UBA5 Asp 106, coordinates an Mg, which occupies similar position to that observed in UBA5 [42]. To test the importance of this Mg site in UBA5, we mutated Asp106 to alanine and tested UFM1 activation. As shown in Fig. 6b and c, this mutation reduced UFM1 activation and accordingly did not abolish the increase of UBA5 thermal stability upon ATP binding. Specifically, an increase in the thermal stability of 12 °C was obtained compared to 17 °C seen with WT UBA5 (Table S2). To further characterize the influence of Asp106 on ATP binding, we measured the affinity of ATP to UBA5 D106A using ITC. As shown in Fig. 6g and Table S1, the data were also best fitted to the two binding sites model, although only one site had a meaningful ratio of ATP to UBA5. This site had a K_d of 500 nM, which is 10-fold higher than the K_d of WT UBA5. Taken together, our data show that the D106A mutation diminishes UBA5's ability to activate UFM1 and to bind ATP. This effect could be due to the inability of Asp106 to coordinate the Mg^{2+}, which in turn contributes to binding and activation. However, we cannot rule out the possibility that the effect of the D106A mutation is structural and is not due to the prevention of the second Mg site.

The significant effect that the N-terminus imposes on how UBA5 interacts with the ATP prompted us to test whether it also affects the spatial structure of ATP. To that end, we superimposed the structures of the short and long isoforms of UBA5 each bound to ATP. As shown in Fig. 6h, in the presence of the N-terminus, the ATP gamma-phosphate is 4.7 Å away from its position in the structure lacking the N-terminus. This movement of the gamma-phosphate prevents clashes with Asn112 that in the structure of the long isoform is no longer flexible as it is in the structure of the short isoform. Interestingly, the structure of ATP that is bound to the long UBA5, but not to the short isoform, is similar to the structure of ATP that is bound to Atg7. Currently, it is unclear whether the structure of ATP that exists in the long isoform provides any benefit to the activation reaction over its structure in the short isoform.

Conclusions

Here we have provided structural and biochemical insights into the contribution of the UBA5 N-terminal extension to UFM1 activation. Previously, we demonstrated that the short UBA5 isoform, lacking the N-terminal extension, executes UFM1's activation in a trans-binding mechanism. Now we have found that while this mechanism is preserved in the long isoform, it is actually improved as the N-terminal extension of one protomer interacts with the adenylation domain of the other protomer as well as with the bound ATP. This not only increases the affinity of UBA5 to ATP but also stabilizes the ATP-bound form of UBA5, thereby stimulating UFM1 activation. Interestingly, even at high ATP concentrations (Fig. 1), the long UBA5 isoform activates UFM1 faster than the short isoform, suggesting that the N-terminal extension contributes not only to the binding of ATP but also to the catalytic process. Indeed, the N-terminal extension stabilizes Arg115 of the adenylation domain, which possesses a catalytic role but makes no contribution to ATP binding (Fig. 6). Taken together, our results suggest that the presence of the N-terminal extension benefits the activation process and enables UFM1 activation under ATP concentrations that do not satisfy activation with the short isoform. Currently, little is known about how the UBA5 isoforms are regulated in the cell, and what cellular benefit accrues from the expression of the short isoform. Indeed, RNA expression analysis of UBA5 isoforms suggests that the long isoform is highly expressed compared to the short isoform [43]. The significant boost the N-terminal extension brings to UFM1 activation raises the question of whether it is regulated in the cell. Previously, it has been shown that Tyr53 of the N-terminus undergoes phosphorylation [44]. In our structure, Tyr53 is 2.5 Å away from Asp141 of the adenylation domain and forms hydrogen bonds with the latter. This therefore suggests that phosphorylation of Tyr53, which provides a negative charge on Tyr53, will prevent interaction with Asp141, thereby interfering with the contribution of the N-terminal extension to UFM1 activation. Overall, our results expand our understanding on UFM1 activation by UBA5 but at the same time call for further investigation of the regulation of UFM1 activation in the cell.

Materials and Methods

Cloning and mutagenesis

Human UBA5, UFM1 and UFC1 were cloned as previously described [34]. UBA5 and UFM1 truncations and mutations were generated either by ligation (T4 DNA Ligase; New England Biolabs) or Gibson

assembly (Gibson assembly master mix; New England Biolabs) according to the manufacturer's protocol. Atg7 and Atg8 (K26P) constructs were amplified as previously described [31].

Protein expression and purification

UBA5, UFM1 and UFC1 were expressed as previously described [34]. In brief, all proteins were expressed in *Escherichia coli T7 express* (New England Biolabs) and grown either in 2xYT (UBA5 constructs) or in Luria–Bertani medium (UFM1 and UFC1 constructs). Cultures were induced at 16 °C overnight with either 0.3 mM (UBA5 constructs) or 0.15 mM (UFM1 and UFC1 constructs) IPTG (T-Fischer BioReagents). Finally, cells were harvested by centrifugation at 6100*g* for 15 min and frozen for further use. For UBA5, UFM1 and UFC1 purification, a protocol earlier described was followed [34]. All proteins were further purified using 16/60 Superdex 75 pg or 16/60 Superdex 200 pg size exclusion chromatography columns (GE Healthcare Life Sciences) equilibrated in buffer containing 20 mM Tris (pH 7.5), 50 mM NaCl and 2 mM DTT. Atg7 and Atg8 K26P were grown and purified as described earlier [31]. Proteins were concentrated and based on their extinction coefficient at 280 nm their concentrations were determined. Finally, they were flash frozen in liquid N_2 and stored at − 80 °C.

Isothermal titration calorimetry

Isothermal titration calorimetry (ITC) experiments were carried out on a MicroCal PEAQ ITC system (Malvern Instruments, Malvern) at 25 °C. The disassociation experiment of UBA5 1–347 was conducted in buffer containing 20 mM Tris (pH 7.5), 50 mM NaCl and 2 mM DTT. UBA5 (440 μM) was titrated to buffer via 19 injections, the volume of each injection was 2 μL with an interval of 120 s. The data were fitted to the disassociation model already built in to the MicroCal PEAQ ITC analysis software. For UFC1 binding to UBA5 1–404 or UBA5 57–404, titration of 2390 μM UFC1 into 239 μM of UBA5 1–404 or UBA5 57–404 was performed in a buffer consisting of 20 mM Tris (pH 7.5), 50 mM NaCl and 2 mM DTT. Measurements were obtained from 19 injections of 2 μL with a spacing of 120 s between each injection. The data were fitted to the two sets of sites model already built in to the MicoCal PEAQ ITC analysis software. The binding experiment of ATP to UBA5 1–347, UBA5 1–346 R55A, UBA5 1–346 R115A or UBA5 1–346 D106A was conducted in a buffer containing 20 mM Tris (pH 7.5), 50 mM NaCl, 2 mM DTT and 5 mM $MgCl_2$. Measurements were obtained from 38 injections of 1 μL with a spacing of 300 s between each injection. The data were fitted to the two sets of sites model already built in to the MicoCal PEAQ ITC analysis software. The initial injection volume in all experiments was 0.4 μL with a duration of 0.8 s. Data for the first injection were not considered in all experiments.

Differential scanning fluorimetry

Differential scanning fluorimetry or TSA was performed with a StepOnePlus real-time PCR system (Applied Biosystems, Life Technologies) using white 96-well plates (Applied Biosystems, Life Technologies) covered with a clear adhesive seal. Assays were performed in a final volume of 25 μL containing 1.6 μM protein, 0 or 5 mM ATP and 7.5× SYPRO Orange (Invitrogen, Life Technologies) mixed in buffer containing 50 mM Bis–Tris (pH 6.5; Sigma Alderich, Merck), 100 mM NaCl and 10 mM $MgCl_2$. Measurements were recorded at an excitation wavelength of 465 nm and an emission wavelength of 580 nm over a temperature rise of 1% from 25 to 90 °C. Each experiment was carried out in triplicates, and the average was obtained for each temperature. The highest and lowest fluorescences were used to normalize the fluorescence intensities. Data were then plotted using GraphPad Prism 6.0 software (La Jolla) and were fitted using Boltzmann sigmoidal curve fit.

Thioester bond formation assay

Charging assay of UBA5 or Atg7: 10 μM UBA5 (WT and mutants) or Atg7 and 20 μM UFM1 or Atg8 was mixed together in a buffer consisting of 50 mM Bis–Tris (pH 6.5), 100 mM NaCl and 10 mM $MgCl_2$. Reactions were initiated by the addition of 5 mM or 10 μM ATP and were incubated at 25 °C. At the designated time point, a sample of the reaction was removed and quenched with SDS sample buffer lacking or containing β-mercaptoethanol (Sigma Alderich, Merck). Samples were then loaded on 12% *Bis-tris* non-reducing SDS-PAGE and visualized by Coomassie brilliant blue R staining.

Charging assay of UFC1 with UFM1: Reactions contained 5 μM UBA5 (1/57–404), 2 μM UFM1 and 5 mM ATP. Reactions were incubated at 30 °C for 30 min before 2 μM of UFC1 was added. Samples were quenched with sample buffer lacking or containing BME and loaded on 12% *Bis-tris* non-reducing SDS-PAGE and visualized by Coomassie brilliant blue R staining.

Size exclusion chromatography with multi-angle light scattering

Assays were performed on an analytical SEC column (Superdex 200 10/300 GL; GE Healthcare Life Sciences) equilibrated with a buffer containing 50 mM Bis–Tris (pH 6.5) and 100 mM NaCl for the analysis of UBA5 lacking the N-terminal extension

(WT and D290K). To obtain the molecular weight of UBA5 containing the N-terminal extension (WT and D290K), the column was equilibrated with buffer containing 20 mM Tris (pH 7.5), 50 mM NaCl and 2 mM DTT. UBA5 – N-terminus ((0.6 mg/mL); WT or D290K) or 0.7 mg/mL of UBA5 + N-terminus (WT or D290K) protein samples were loaded on an HPLC, which was connected to 18-angle light-scattering detector, followed by a differential refractive index detector (Wyatt Technology). Molecular mass within a defined chromatographic peak was calculated using ASTRA software, version 7 (Wyatt Technologies).

Cross-linking of UBA5 with UFM1 G83C

The purified protein UFM1 G83C was desalted in PBS buffer by loading on to the desalting column Sephadex G 25 (GE Health Care Life Sciences) pre-equilibrated with PBS buffer. The fractions eluted from the desalting column corresponding to the peak were pooled and concentrated to 100 μM. To activate the UFM1 G83C with the cross-linker, a reaction was setup by adding BMOE (Thermo Scientific) to a final concentration of 400 μM to 100 μM UFM1 G83C, in order to maintain a 1:4 ratio between UFM1 G83C and BMOE. The stock of BMOE (20 mM) was prepared by dissolving it in 100% DMSO. The reaction was incubated for 1 h at room temperature in a dark place. The activated UFM1 G83C was then loaded on to the Sephadex G 25 desalting column equilibrated with PBS buffer in order to remove the unreacted BMOE. The fractions corresponding to the peak were pooled and concentrated using an Amicon Ultra-15 centrifugal filtration device with an MW cutoff of 3 kDa (Millipore, Merck). The concentrated UFM1 G83C activated with BMOE was flash frozen in liquid nitrogen until further use. For the cross-linking reaction, 2 μM of UBA5 (1/57–404) was mixed with 5 μM of UFM1 G83C-BMOE in PBS buffer and incubated for 30 min at 20 °C. The reaction was then concentrated and loaded on to a Superdex 200 10/300GL analytical sizing column (GE Health Care, Life Sciences). The fractions corresponding to the peak were pooled and concentrated using an Amicon Ultra-15 centrifugal filtration device (Millipore, Merck) with an MW cutoff of 10 kDa.

Crystallization

All crystals were grown at 20 °C using the hanging drop vapor diffusion method. UBA5 37–335 (32.6 mg/mL) was mixed with 2 mM ATP and 5 mM $MgCl_2$ followed by incubation on ice for 15 min. Crystals appeared within 4 days in solution containing 0.2 M sodium citrate tribasic dehydrate (pH 7.9) and 20% PEG 3350. Crystals of UBA5-UFM1 complex were prepared by mixing 22.8 mg/mL UBA5 37–347 and 9.32 mg/mL UFM1 1–78 in a molar ratio of 1:1 along with 2 mM ATP and 5 mM $MgCl_2$. The mixture was incubated for 15 min on ice. Crystals appeared within 4 days in a solution containing 0.2 M lithium nitrate (pH 7.1), 21% PEG 3350, 0.2 M magnesium chloride hexahydrate and 35% v/v pentaerythritol ethoxylate (3/4 EO/OH). All crystals were cryo-protected using reservoir solution comprising 30% glycerol and flash frozen in liquid nitrogen.

X-ray data collection and processing

Initial UBA5–ATP data were collected at beamline ID29, ESRF. The data were processed using XDS [45] to 2.65 Å in the trigonal space group $P3_2$ and were found to be twinned with a twin fraction close to 50% [46]. The twinning affected the downstream structure refinement; therefore, more than 50 crystals were screened at ID30A-1, ESRF in search for either a non-twinned crystal or the one with a lower twin fraction. A single crystal belonged in a different monoclinic group $P2_1$, for which 163° of data was collected with 0.05° increment. These monoclinic data showed apparent radiation damage for the last quarter of the images. Therefore data from images 1–2400 to 2.7-Å resolution and data from images 2401–3260 to 6 Å were processed by XDS, merged and scaled together to maintain completeness at low resolution. UBA5–UFM1 data were collected on ID29, ESRF and processed to 2.1 Å by DIALS [47] within the XIA2 pipeline [48].

Structure determination

The structure of UBA5–ATP was originally solved in the $P3_2$ space group by MR method using a single monomer of pdb 3H8V (residues 69–318 of UBA5) [21] as a model. Although the rotation function calculated in MOLREP [49] at 2.7-Å resolution had poor contrast, the translation search at 3-Å resolution easily positioned four monomers of UBA5, which comprise the asymmetric unit of this crystal form. The rotation function solutions proved to be within the first 10 peaks. The model was refined in REFMAC5 [50] and rebuilt in COOT [51]. Residues 45–68 absent in the model were positioned; however, due to twinning, the quality of electron density maps was poor even when *R*-factors in REFMAC5 twin refinement were low. This partially refined structure was used as a model to position 16 monomers of UBA5 (37–347) in the monoclinic space group. The 16-fold NCS averaging implemented in DM [52] was used for phase improvement at initial stages, with density modification phases input for phase refinement [53] in REFMAC5. At a later stage, the UBA5 was separated into four groups of four monomers on the basis of conformation of region 230–251. Masks and NCS operators were found within each group and 4-fold averaging was used for density improvement.

The refined structure of UBA5–ATP (37–335) was used as a model for solution of UBA5–UFM1–ATP complex. Four monomers of UBA5 were positioned with high contrast by MOLREP. Four UFM1 monomers were positioned by MOLREP with UBA5 used as fixed model.

Mg ions were originally observed coordinating ATP at two positions in the twinned UBA5–ATP structure. In the higher resolution UBA5–UFM1–ATP, two positions for Mg ions that were octahedrally coordinated by oxygens of ATP, protein side chains and waters were clearly visible in all monomers. Two Mg ions per ATP and some coordinating waters were also visible in the monoclinic space group, but were less ordered due to low resolution and radiation damage.

Structure deposition

The atomic coordinates and structure factors were deposited in the Protein Data Bank with accession numbers of 6H77 and 6H78 for the structures of UBA5 with and without UFM1, respectively.

Supplementary data to this article can be found online at https://doi.org/10.1016/j.jmb.2018.10.007.

Acknowledgements

We thank the staff of beamlines ID29 and ID30A-1 of the European Synchrotron Radiation Facility. This work was supported by, the Marie Curie Career Integration Grant (PCIG13-GA-2013-630755), the Israel Science Foundation (Grant 1383/17) and the Israeli Cancer Association (Grant 20180069).

Author Contributions: N.S. and R.W. designed the experiments, and N.S., and M.K performed all biochemical experiments. Cloning, expression and protein purification were carried out by N.S., E.C.K., B. M. and F.H. Complexes were prepared for crystallization, and crystals were grown by N.S. and P.P. M.I., A.L., P.P. and R.W. determined the crystal structures. N.S., P.P. and R.W. wrote the manuscript.

Conflict of Interest Statement: The authors declare no conflicts of interest.

Received 30 August 2018;
Received in revised form 15 October 2018;
Accepted 17 October 2018
Available online 6 November 2018

Keywords
UFM1;
UBA5;
ubiquitin-like proteins;
E1 activating enzymes;
crystal structure

Abbreviations used:
UFM1, ubiquitin fold modifier 1; UBA5, ubiquitin-like modifier-activating enzyme 5; UFC1, ubiquitin-fold modifier-conjugating enzyme 1; UIS, UFM1-interacting sequence; ITC, isothermal titration calorimetry; TSA, thermal shift assay; BMOE, bis-maleimidoethane.

References

[1] M. Komatsu, T. Chiba, K. Tatsumi, S. Iemura, I. Tanida, N. Okazaki, et al., A novel protein-conjugating system for Ufm1, a ubiquitin-fold modifier, EMBO J. 23 (2004) 1977–1986.
[2] P. Padala, W. Oweis, B. Mashahreh, N. Soudah, E. Cohen-Kfir, E.A. Todd, et al., Novel insights into the interaction of UBA5 with UFM1 via a UFM1-interacting sequence, Sci. Rep. 7 (2017).
[3] H. Sasakawa, E. Sakata, Y. Yamaguchi, M. Komatsu, K. Tatsumi, E. Kominami, et al., Solution structure and dynamics of Ufm1, a ubiquitin-fold modifier 1, Biochem. Biophys. Res. Commun. 343 (2006) 21–26.
[4] A. Azfer, J. Niu, L.M. Rogers, F.M. Adamski, P.E. Kolattukudy, Activation of endoplasmic reticulum stress response during the development of ischemic heart disease, Am. J. Physiol. Heart Circ. Physiol. 291 (2006) H1411–H1420.
[5] Y. Cai, W. Pi, S. Sivaprakasam, X. Zhu, M. Zhang, J. Chen, et al., UFBP1, a key component of the Ufm1 conjugation system, is essential for ufmylation-mediated regulation of erythroid development, PLoS Genet. 11 (2015), e1005643.
[6] Y. Cai, N. Singh, H. Li, Essential role of Ufm1 conjugation in the hematopoietic system, Exp. Hematol. 44 (2016) 442–446.
[7] J. Daniel, E. Liebau, The ufm1 cascade, Cell 3 (2014) 627–638.
[8] P. Hertel, J. Daniel, D. Stegehake, H. Vaupel, S. Kailayangiri, C. Gruel, et al., The ubiquitin-fold modifier 1 (Ufm1) cascade of Caenorhabditis elegans, J. Biol. Chem. 288 (2013) 10661–10671.
[9] K. Lemaire, R.F. Moura, M. Granvik, M. Igoillo-Esteve, H.E. Hohmeier, N. Hendrickx, et al., Ubiquitin fold modifier 1 (UFM1) and its target UFBP1 protect pancreatic beta cells from ER stress-induced apoptosis, PLoS One 6 (2011), e18517.
[10] L. Pirone, W. Xolalpa, J.O. Sigurethsson, J. Ramirez, C. Perez, M. Gonzalez, et al., A comprehensive platform for the analysis of ubiquitin-like protein modifications using in vivo biotinylation, Sci. Rep. 7 (2017) 40756.
[11] M. Zhang, X. Zhu, Y. Zhang, Y. Cai, J. Chen, S. Sivaprakasam, et al., RCAD/Ufl1, a Ufm1 E3 ligase, is essential for hematopoietic stem cell function and murine hematopoiesis, Cell Death Differ. 22 (2015) 1922–1934.
[12] E. Colin, J. Daniel, A. Ziegler, J. Wakim, A. Scrivo, T.B. Haack, et al., Biallelic variants in UBA5 reveal that disruption of the UFM1 cascade can result in early-onset encephalopathy, Am. J. Hum. Genet. 99 (2016) 695–703.
[13] C. Mignon-Ravix, M. Milh, C.S. Kaiser, J. Daniel, F. Riccardi, P. Cacciagli, et al., Abnormal function of the UBA5 protein in a case of early developmental and epileptic encephalopathy with suppression-burst, Hum. Mutat. 39 (2018) 934–938.
[14] M. Muona, R. Ishimura, A. Laari, Y. Ichimura, T. Linnankivi, R. Keski-Filppula, et al., Biallelic variants in UBA5 link dysfunctional UFM1 ubiquitin-like modifier pathway to severe infantile-onset encephalopathy, Am. J. Hum. Genet. 99 (2016) 683–694.
[15] M.S. Nahorski, S. Maddirevula, R. Ishimura, S. Alsahli, A.F. Brady, A. Begemann, et al., Biallelic UFM1 and UFC1

mutations expand the essential role of ufmylation in brain development, Brain 141 (2018) 1934–1945.
[16] H.M. Yoo, S.H. Kang, J.Y. Kim, J.E. Lee, M.W. Seong, S.W. Lee, et al., Modification of ASC1 by UFM1 is crucial for ERalpha transactivation and breast cancer development, Mol. Cell 56 (2014) 261–274.
[17] K. Tatsumi, H. Yamamoto-Mukai, R. Shimizu, S. Waguri, Y.S. Sou, A. Sakamoto, et al., The Ufm1-activating enzyme Uba5 is indispensable for erythroid differentiation in mice, Nat. Commun. 2 (2011) 181.
[18] A.D. Capili, C.D. Lima, Taking it step by step: mechanistic insights from structural studies of ubiquitin/ubiquitin-like protein modification pathways, Curr. Opin. Struct. Biol. 17 (2007) 726–735.
[19] L. Cappadocia, C.D. Lima, Ubiquitin-like protein conjugation: structures, chemistry, and mechanism, Chem. Rev. 118 (2018) 889–918.
[20] C.M. Pickart, M.J. Eddins, Ubiquitin: structures, functions, mechanisms, Biochim. Biophys. Acta 1965 (2004) 55–72.
[21] J.P. Bacik, J.R. Walker, M. Ali, A.D. Schimmer, S. Dhe-Paganon, Crystal structure of the human ubiquitin-activating enzyme 5 (UBA5) bound to ATP: mechanistic insights into a minimalistic E1 enzyme, J. Biol. Chem. 285 (2010) 20273–20280.
[22] T. Mizushima, K. Tatsumi, Y. Ozaki, T. Kawakami, A. Suzuki, K. Ogasahara, et al., Crystal structure of Ufc1, the Ufm1-conjugating enzyme, Biochem. Biophys. Res. Commun. 362 (2007) 1079–1084.
[23] K. Tatsumi, Y.S. Sou, N. Tada, E. Nakamura, S. Iemura, T. Natsume, et al., A novel type of E3 ligase for the Ufm1 conjugation system, J. Biol. Chem. 285 (2010) 5417–5427.
[24] B.A. Schulman, J.W. Harper, Ubiquitin-like protein activation by E1 enzymes: the apex for downstream signalling pathways, Nat. Rev. Mol. Cell Biol. 10 (2009) 319–331.
[25] S.B. Hong, B.W. Kim, K.E. Lee, S.W. Kim, H. Jeon, J. Kim, et al., Insights into noncanonical E1 enzyme activation from the structure of autophagic E1 Atg7 with Atg8, Nat. Struct. Mol. Biol. 18 (2011) 1323–1330.
[26] M.W. Lake, M.M. Wuebbens, K.V. Rajagopalan, H. Schindelin, Mechanism of ubiquitin activation revealed by the structure of a bacterial MoeB–MoaD complex, Nature 414 (2001) 325–329.
[27] N.N. Noda, K. Satoo, Y. Fujioka, H. Kumeta, K. Ogura, H. Nakatogawa, et al., Structural basis of Atg8 activation by a homodimeric E1, Atg7, Mol. Cell 44 (2011) 462–475.
[28] A.M. Taherbhoy, S.W. Tait, S.E. Kaiser, A.H. Williams, A. Deng, A. Nourse, et al., Atg8 transfer from Atg7 to Atg3: a distinctive E1–E2 architecture and mechanism in the autophagy pathway, Mol. Cell 44 (2011) 451–461.
[29] S. Habisov, J. Huber, Y. Ichimura, M. Akutsu, N. Rogova, F. Loehr, et al., Structural and functional analysis of a novel interaction motif within UFM1-activating enzyme 5 (UBA5) required for binding to ubiquitin-like proteins and ufmylation, J. Biol. Chem. 291 (2016) 9025–9041.
[30] S. Xie, Characterization, crystallization and preliminary X-ray crystallographic analysis of the Uba5 fragment necessary for high-efficiency activation of Ufm1, Acta Crystallogr F Struct Biol Commun 70 (2014) 765–768.
[31] B. Mashahreh, F. Hassouna, N. Soudah, E. Cohen-Kfir, R. Strulovich, Y. Haitin, et al., Trans-binding of UFM1 to UBA5 stimulates UBA5 homodimerization and ATP binding, FASEB J. 32 (2018) 2794–2802 (fj201701057R).
[32] S. Xie, Characterization, crystallization and preliminary X-ray crystallographic analysis of the human Uba5 C-terminus–Ufc1 complex, Acta Crystallogr F Struct Biol Commun 70 (2014) 1093–1097.
[33] M. Zheng, X. Gu, D. Zheng, Z. Yang, F. Li, J. Zhao, et al., UBE1DC1, an ubiquitin-activating enzyme, activates two different ubiquitin-like proteins, J. Cell. Biochem. 104 (2008) 2324–2334.
[34] W. Oweis, P. Padala, F. Hassouna, E. Cohen-Kfir, D.R. Gibbs, E.A. Todd, et al., Trans-binding mechanism of ubiquitin-like protein activation revealed by a UBA5–UFM1 complex, Cell Rep. 16 (2016) 3113–3120.
[35] C. Berezin, F. Glaser, J. Rosenberg, I. Paz, T. Pupko, P. Fariselli, et al., ConSeq: the identification of functionally and structurally important residues in protein sequences, Bioinformatics 20 (2004) 1322–1324.
[36] Z. Tokgoz, R.N. Bohnsack, A.L. Haas, Pleiotropic effects of ATP.Mg^{2+} binding in the catalytic cycle of ubiquitin-activating enzyme, J. Biol. Chem. 281 (2006) 14729–14737.
[37] A.L. Haas, I.A. Rose, The mechanism of ubiquitin activating enzyme. A kinetic and equilibrium analysis, J. Biol. Chem. 257 (1982) 10329–10337.
[38] J.M. Gavin, K. Hoar, Q. Xu, J. Ma, Y. Lin, J. Chen, et al., Mechanistic study of Uba5 enzyme and the Ufm1 conjugation pathway, J. Biol. Chem. 289 (2014) 22648–22658.
[39] S.E. Kaiser, K. Mao, A.M. Taherbhoy, S. Yu, J.L. Olszewski, D.M. Duda, et al., Noncanonical E2 recruitment by the autophagy E1 revealed by Atg7–Atg3 and Atg7–Atg10 structures, Nat. Struct. Mol. Biol. 19 (2012) 1242–1249.
[40] L.M. Lois, C.D. Lima, Structures of the SUMO E1 provide mechanistic insights into SUMO activation and E2 recruitment to E1, EMBO J. 24 (2005) 439–451.
[41] H. Walden, M.S. Podgorski, D.T. Huang, D.W. Miller, R.J. Howard, D.L. Minor Jr., et al., The structure of the APPBP1–UBA3–NEDD8–ATP complex reveals the basis for selective ubiquitin-like protein activation by an E1, Mol. Cell 12 (2003) 1427–1437.
[42] S.K. Olsen, C.D. Lima, Structure of a ubiquitin E1–E2 complex: insights to E1–E2 thioester transfer, Mol. Cell 49 (2013) 884–896.
[43] I.S. Yang, H. Son, S. Kim, S. Kim, ISOexpresso: a web-based platform for isoform-level expression analysis in human cancer, BMC Genomics 17 (2016) 631.
[44] Y. Bai, J. Li, B. Fang, A. Edwards, G. Zhang, M. Bui, et al., Phosphoproteomics identifies driver tyrosine kinases in sarcoma cell lines and tumors, Cancer Res. 72 (2012) 2501–2511.
[45] W. Kabsch, Xds, Acta Crystallogr. Sect. D: Biol. Crystallogr. 66 (2010) 125–132.
[46] A.A. Vaguine, J. Richelle, S.J. Wodak, SFCHECK: a unified set of procedures for evaluating the quality of macromolecular structure-factor data and their agreement with the atomic model, Acta Crystallogr. D Biol. Crystallogr. 55 (1999) 191–205.
[47] D.G. Waterman, G. Winter, R.J. Gildea, J.M. Parkhurst, A.S. Brewster, N.K. Sauter, et al., Diffraction-geometry refinement in the DIALS framework, Acta Crystallogr D Struct Biol 72 (2016) 558–575.
[48] G. Winter, C.M. Lobley, S.M. Prince, Decision making in xia2, Acta Crystallogr. D Biol. Crystallogr. 69 (2013) 1260–1273.
[49] A. Vagin, A. Teplyakov, Molecular replacement with MOLREP, Acta Crystallogr. D Biol. Crystallogr. 66 (2010) 22–25.
[50] G.N. Murshudov, P. Skubak, A.A. Lebedev, N.S. Pannu, R.A. Steiner, R.A. Nicholls, et al., REFMAC5 for the refinement of macromolecular crystal structures, Acta Crystallogr. D Biol. Crystallogr. 67 (2011) 355–367.

[51] P. Emsley, K. Cowtan, Coot: model-building tools for molecular graphics, Acta Crystallogr. D Biol. Crystallogr. 60 (2004) 2126–2132.
[52] K. Cowtan, Recent developments in classical density modification, Acta Crystallogr. D 66 (2010) 470–478.
[53] N.S. Pannu, G.N. Murshudov, E.J. Dodson, R.J. Read, Incorporation of prior phase information strengthens maximum-likelihood structure refinement, Acta Crystallogr. D 54 (1998) 1285–1294.